

Article

Numerical Study of Meteorological Factors for Tropospheric Nocturnal Ozone Increase in the Metropolitan Area of São Paulo

Viviana Vanesa Urbina Guerrero¹, Marcos Vinicius Bueno de Moraes^{2,*} , Edmilson Dias de Freitas¹ 
and Leila Droprinchinski Martins³ 

- ¹ Instituto de Astronomia, Geofísica e Ciências Atmosféricas, Universidade de São Paulo, São Paulo 05508-090, Brazil; viviana.urbina@gmail.com (V.V.U.G.); edmilson.freitas@iag.usp.br (E.D.d.F.)
² Departamento de Obras Civiles, Facultad de Ciencias de la Ingeniería, Universidad Católica del Maule, Av. San Miguel, 3605, Talca 3480112, Chile
³ Department of Chemistry, Federal University of Technology—Paraná, Pioneiros Avenue, 3131, Londrina 86036-370, Brazil; leilamartins@utfpr.edu.br
* Correspondence: bmarcos@ucm.cl; Tel.: +56-712-203-566

Abstract: One of the central problems in large cities is air pollution, mainly caused by vehicular emissions. Tropospheric ozone is an atmospheric oxidizing gas that forms in minimal amounts naturally, affecting peoples' health. This pollutant is formed by the NO₂ photolysis, creating a main peak during the day. Nighttime secondary peaks occur in several parts of the world, but their intensity and frequency depend on the local condition. In this sense, this work aims to study the local characteristics for tropospheric nocturnal ozone levels in the Metropolitan Area of São Paulo, in Brazil, using the Simple Photochemical Module coupled to the Brazilian Developments on the Regional Atmospheric Modeling System. For this, three different situations of nocturnal occurrence were studied. The results show that the nocturnal maximum of ozone concentrations is related to the vertical transport of this pollutant from higher levels of the atmosphere to the surface and is not related to the synoptic condition.

Keywords: air quality modeling; BRAMS; nighttime ozone



Citation: Urbina Guerrero, V.V.; Moraes, M.V.B.d.; Freitas, E.D.d.; Martins, L.D. Numerical Study of Meteorological Factors for Tropospheric Nocturnal Ozone Increase in the Metropolitan Area of São Paulo. *Atmosphere* **2021**, *12*, 287. <https://doi.org/10.3390/atmos12020287>

Academic Editor: Anthony R. Lupo

Received: 2 February 2021
Accepted: 19 February 2021
Published: 23 February 2021

Publisher's Note: MDPI stays neutral with regard to jurisdictional claims in published maps and institutional affiliations.



Copyright: © 2021 by the authors. Licensee MDPI, Basel, Switzerland. This article is an open access article distributed under the terms and conditions of the Creative Commons Attribution (CC BY) license (<https://creativecommons.org/licenses/by/4.0/>).

1. Introduction

In recent years, large cities' main problem is excessive air pollution, resulting in several economic and public health problems [1–4]. In Latin America, urban centers are in constant development and growth, generating numerous problems associated with the effects of pollution [5,6]. In general, the primary source of air pollution for large cities is vehicular, while small and medium-sized cities have industrial sources [7]. Besides the relevance of emission sources, several studies have shown that the meteorological condition greatly influences pollutants' concentrations [8–13].

Tropospheric ozone (O₃) is an atmospheric oxidizing gas that forms in minimal amounts naturally. This secondary photochemical pollutant is formed in the atmosphere by photodissociation of nitrogen dioxide (NO₂) by ultra-violet light. Being an oxidant pollutant, ground-level ozone concentration can affect people's health (especially children, the elderly, and people in outdoor activities), worsen pre-existent diseases and increasing hospitalizations for respiratory diseases in risk groups [14]. Also, ozone exposure can be related to morbidity and mortality from cardiopulmonary diseases [15]. In the United States, ozone contributes to increasing the mortality rate associated with respiratory diseases; an increment of 10 ppb in ground-level concentrations increases by 3% death risk associated with exposure [16]. Climatic change could be responsible for increasing ozone concentrations and, consequently, for the number of hospital admissions and deaths associated with ozone exposure [4]. Since the change in ozone concentrations is a consequence of changes

in the atmospheric system, it is essential to know which synoptic patterns are associated with particular conditions of ground-level ozone concentrations.

During the night, in very stable situations, especially under anticyclonic conditions, the increase of this contaminant has been observed with a well-defined behavior [17]. In cyclonic conditions, NO_x can have a low concentration due to increased ventilation and affect O₃ concentration [18]. The magnitude and frequency of nocturnal ozone peaks are generally observed in the summertime and associated with horizontal transport processes [19]. In China, the nocturnal O₃ concentration is higher in suburban areas than that in urban areas before a nocturnal O₃ increase, the contrast being reduced under vertical transport [20]. Also, in Kolkata, India, the nocturnal ozone mean concentrations increased in urban and suburban areas, where NO_x plays a critical role through O₃-NO-NO₂ chemistry [21]. The reduction in NO_x emissions (by road traffic control strategies) produces substantial changes in nighttime ozone in urban areas [22,23], with higher ozone concentrations due to a lower gas-phase titration of ozone with NO.

Given the importance and the elements that influence the magnitude and frequency of nocturnal ozone, this work aims to study the local characteristics of the atmosphere of the Metropolitan Area of São Paulo (MASP) in the formation of secondary ozone peaks during the night. For this, regional numerical modeling, with a mesoscale atmospheric model coupled with a chemical module, was used.

2. Materials and Methods

2.1. Study Area

The MASP is located in southeastern Brazil, in a region of rugged topography (Figure 1), in which the city of São Paulo is located in the most central region coinciding with the valleys of the Tietê and Pinheiros rivers, between Serra do Mar and Serra da Cantareira, the latter with elevations above 1000 m. The MASP comprises 39 municipalities and concentrates almost half of the state's total population (approximately 20 million inhabitants), covering an area of 8051 km² [24].

Given the proximity to the sea and the surface extension of the built-up area, the Urban Heat Island (UHI) effect significantly influences the flow patterns [25] in dispersing pollutants. The passage of the sea breeze creates a favorable condition for the dispersion of pollutants in this urban region, while days with extreme UHI events generate a more stable condition in the MASP, which may favor the accumulation of pollutants [12]. In winter and early spring, there is a greater frequency of days with the high-pressure systems that hinder the passage of cold fronts, favoring the formation of a high-intensity UHI, which generates more appropriate conditions for the occurrence of high pollutant concentration events [26].

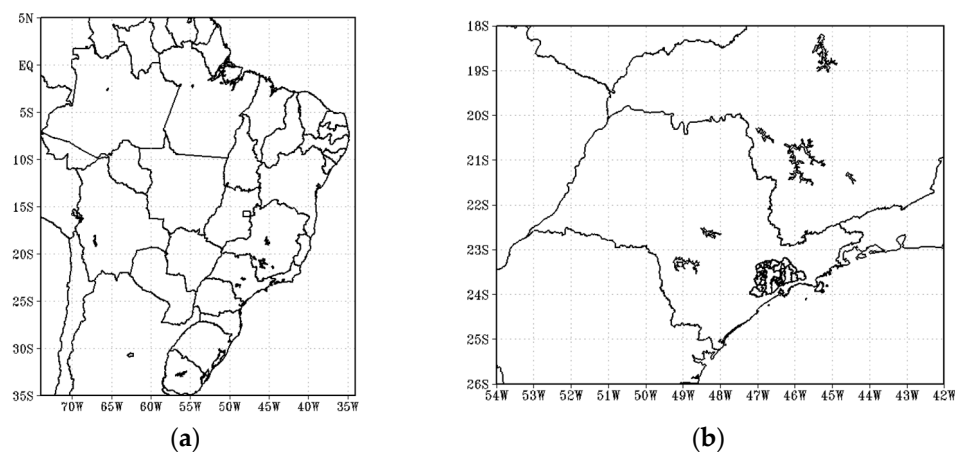


Figure 1. Cont.

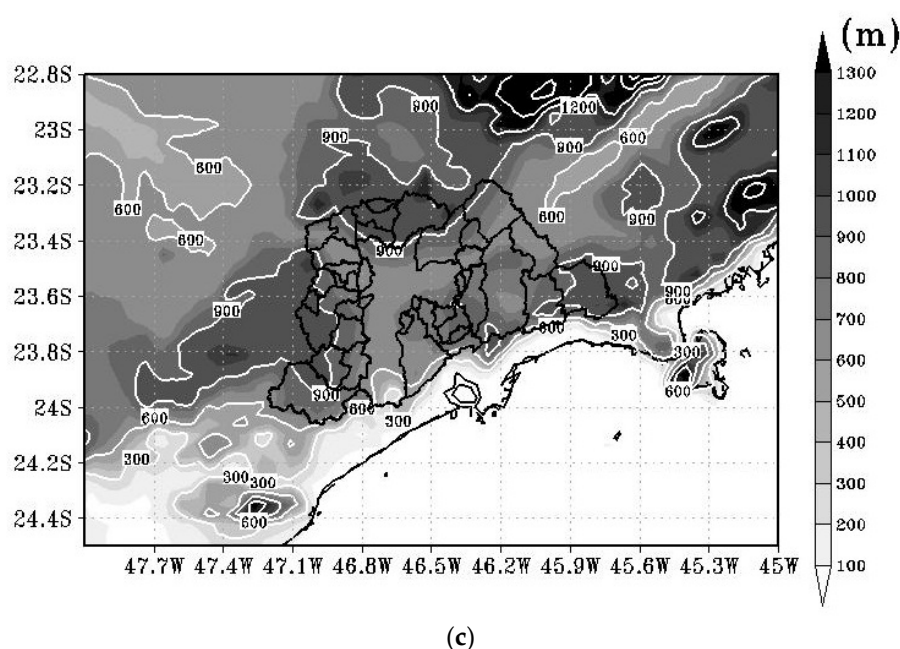


Figure 1. (a) Location, (b) cities and (c) topography map (scale bar in meters). Cities of the Metropolitan Area of São Paulo (MASP) are in the solid black line. Topography data set from United States Geological Survey (USGS).

2.2. SPM-BRAMS

Version 3.2 of the BRAMS model (Brazilian Development on Regional Atmospheric Modeling System, [27]) was used in this work. This model is based on the Regional Atmospheric Modeling System (RAMS, [28]), which simulates several spatial scales, integrating the microscale with the larger scales. The equations system that governs the atmospheric state is solved using second-order finite difference schemes, both in time and space. Numerical instability is minimized by using smaller time steps in solving equations in higher resolution grids. Atmospheric physical processes are considered by several parameterizations. The model has a multiple grid scheme that allows the simultaneous solution of the equations. The interaction processes between the surface and atmosphere are carried out in BRAMS using the LEAF-3 model (Land Ecosystem-Atmosphere Feedback model version 3, [29]) for vegetated areas and using TEB (Town Energy Budget, [30]) for urban areas.

Figure 2 presents the nesting grids used in the simulations centered at the MASP (-23.60° , -46.65°). The horizontal grid spacing of both domains are 16 and 4 km, from lower to the higher resolution. The topography is based on the United States Geological Survey (USGS) data set with 1 km of the horizontal spacing grid. For the seawater surface temperature, weekly mean values corresponding to the simulated periods were used as input data, without considering the update of these files during the integration. As a meteorological initial condition, the Global Forecasting System (GFS) global model's outputs with a horizontal grid spacing of 1° were used. For all analysis of the results, the simulations were run one day before the nocturnal event, and we rejected the first 24 h to avoid the spin-up effect [31] of the meteorological part of the model and also to allow the model to accumulate more realistic amounts of pollutants in the atmosphere. The first level of the model output considered was 33.4 m above the surface. The model physics and land-use parameterization configuration are the same as in Morais et al. [32].

The Simple Photochemical Module (SPM, [33]) was inserted in the BRAMS model to generate operational forecasts of ozone concentrations and other constituents for the MASP with a reduced number of chemical reactions. Ozone formation was represented without considering hydrocarbon speciation. The relevant reactions were selected from the chemical mechanism SAPRC-99, which in turn was used in the CIT photochemical model (Caltech Institute of Technology, [34]). Volatile organic compounds were considered

in a single category to simplify the numerical scheme and reduce the integration time. The emissions module consisted of an Eulerian dispersion model integrating the mass conservation equation, which distributed the emission. For the vehicular contribution, the emissions were distributed in space and time within the grid following a daily cycle based on a double Gaussian distribution to represent the periods with the highest vehicular flow. The module also made an adjustment to consider variations in emissions during the weekdays and on weekends.

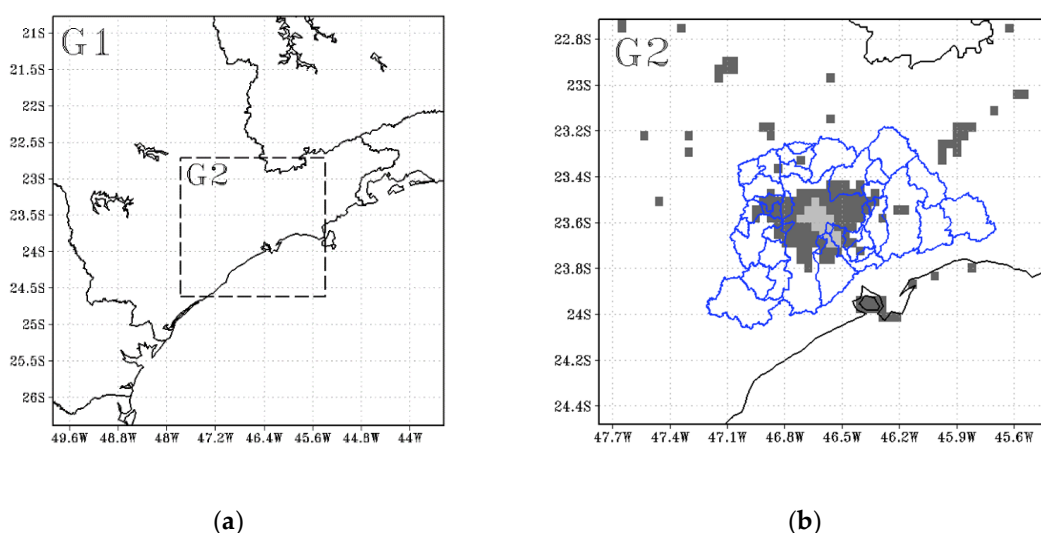


Figure 2. Grid domains used in the simulation. (a) Lower resolution domain (G1), and (b) higher resolution. Lighter gray color represents the dense urban area since dark gray is the suburban area (similar to Morais et al. [32]).

2.3. Model Evaluation

Two statistical indices were used to assess the proximity of the result generated by the model with the observed values of O_3 in the MASP. Bias measures the model's tendency to underestimate or overestimate the value of a variable with its observed value and is defined by the expression

$$\text{BIAS} = \frac{1}{N} \sum_{i=1}^N (S_i - O_i), \quad (1)$$

where S_i corresponds to the i -th value of the simulated variable, and O_i for the same observed variable. N is the total number of data.

The Root Mean Square Error (RMSE) was used to express the accuracy of the numerical results and is given by the following equation

$$\text{RMSE} = \frac{1}{N} \sum_{i=1}^N \sqrt{(S_i - O_i)^2}, \quad (2)$$

where S_i corresponds to the i -th value of the simulated variable, and O_i for the same observed variable. N is the number of data.

Air quality stations from the Companhia Ambiental do Estado de São Paulo (CETESB) were chosen to assess the model's performance in representing the concentration levels close to the surface (Figure 3). For meteorological variables, the model was extensively validated by Morais et al. [32,35]. The period of model evaluation started at 21:00 Local Time on 26 August 2010, with 72 h of simulation that corresponded to a high-level of ozone concentration event resulting from an extensive drought period without rain events [36].

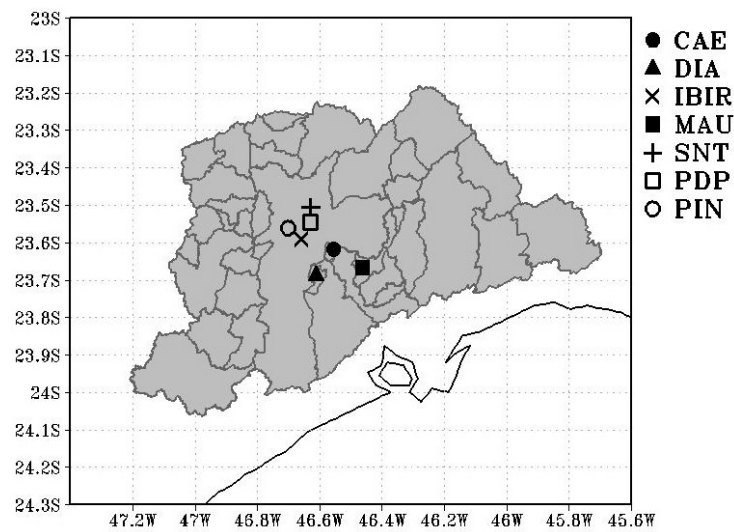


Figure 3. Location of CETESB’s monitoring network stations in the Metropolitan Region of São Paulo (in gray) used for this study, where CAE corresponds to São Caetano do Sul station, DIA to Diadema station, IBIR to Parque do Ibirapuera station, MAU to Mauá station, SNT to Santana station, PDP to Parque Dom Pedro II station and PIN to Pinheiros station.

2.4. Experimental Design

Three different periods were considered to study the local meteorological factors that influence the increase in nocturnal ozone concentration. The first one corresponded to the condition where the nighttime ozone increase was recorded in all stations (case 7E), which occurred on 25 December 2010. The second was a period where no nocturnal ozone was recorded in any selected stations (case 0E), which was on 22 January 2005. The third simulation (named here as case GP) represented a case with three high-level events in the São Caetano do Sul (CAET), Diadema (DIAD), and Mauá (MAUA) stations, which occurred on 12 October 2001.

Figure 4 shows the synoptic patterns for 0E and 7E at 00:00 and 06:00 UTC. These data were obtained from the NCEP/NCAR reanalysis [37]. The synoptical pattern analyzed in both times did not change, and only a displacement from the high pressure, at both levels, to the ocean was observed. When analyzing the reduced pressure at sea level (Figure 5), the South Atlantic Subtropical Anticyclone (SASA) was observed to be more intense and closer to the coast of southeastern Brazil than in the case where nightly ozone increase was recorded. In both cases, SASA shift to the east was observed at the immediately higher levels of the atmosphere.

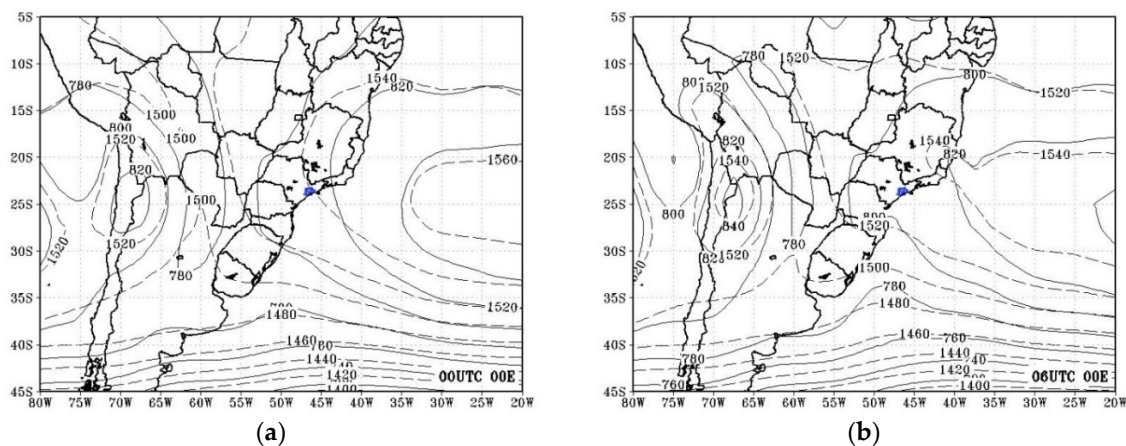


Figure 4. Cont.

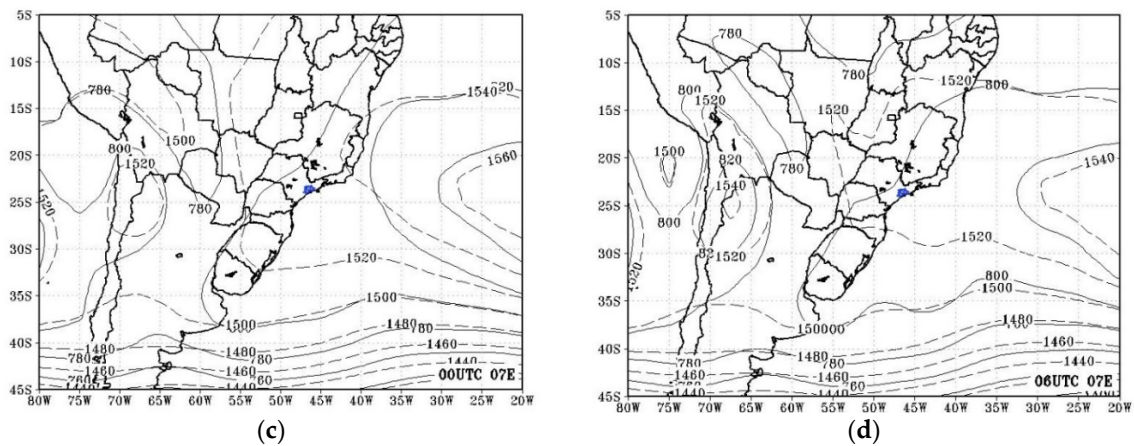


Figure 4. Geopotential height (in m) in the 850 hPa (dashed line) and 925 hPa (continuous line) for 0E case at (a) 00:00 and (b) 06:00 UTC, and for 7E case at (c) 00:00 and (d) 06:00 UTC. MASP is colored in blue.

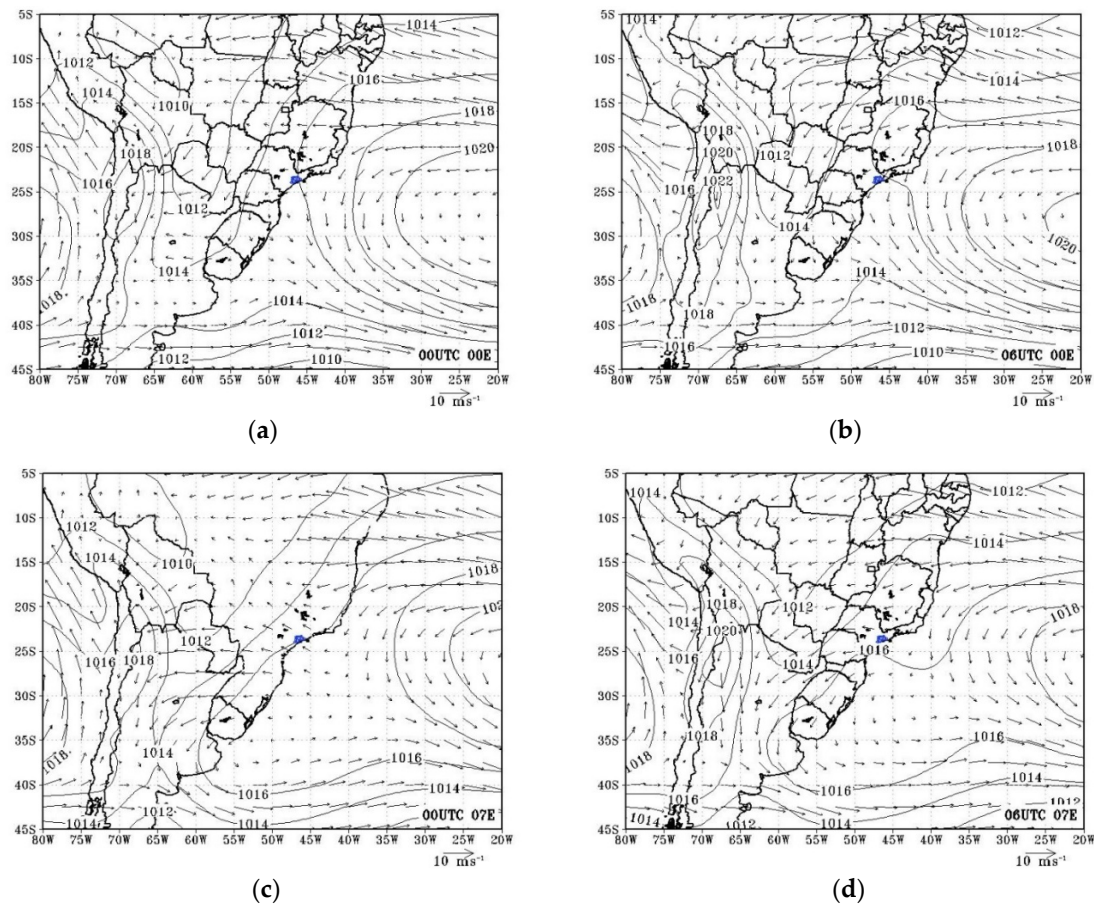


Figure 5. Contour lines of sea level pressure (in hPa) and wind field (in m s^{-1}) in 925 hPa for 0E case at (a) 00:00 and (b) 06:00 UTC, and for 7E case at (c) 00:00 and (d) 06:00 UTC. MASP is colored in blue.

The discussion is done by analyzing the O_3 evolution for each station and by an average nocturnal concentration map. After, a vertical profile of the ozone is analyzed, considering the latitude of MASP.

3. Results

3.1. Model Evaluation

Figure 6 shows the RMSE and bias scatter plot of the ozone concentration for all available air quality stations in the MASP. Based on the bias, it appears that the model

tended to underestimate the values of O_3 . The absolute value of these indices is related to the order of magnitude of the variable. However, it appears that the values were like those obtained by other authors [9,38]. Besides, it is noted that the Ibirapuera park station had the worst rates, which may be related to the intense presence of green areas in the place, needing to improve this type of representation in the model [35].

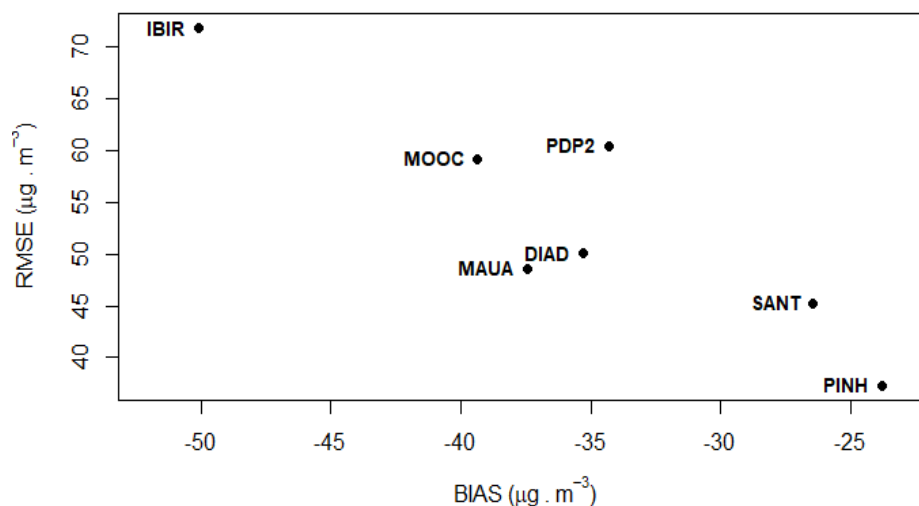


Figure 6. Root mean square error (RMSE) versus bias for ozone concentration. Each point represents an air quality station Pinheiros (PINH) and Santana (SANT).

3.2. Nocturnal Ozone Experiments

3.2.1. No Increase in Ozone Concentration (0E)

Figure 7 shows the concentrations simulated by the model for air quality stations in cases where no increase in ozone concentration was observed during the night (0E, left column). In the 0E case, the model represented the behavior of nocturnal concentrations relatively well, with the diurnal peak being underestimated, especially on the second day. The mean ozone field and reduced pressure at mean sea level (Figure 8) showed an anticyclone located southeast of the simulation domain, which concentrated the core of maximum ozone concentration values. Values below $36 \mu\text{g m}^{-3}$ were observed in almost the entire continental part. The pressure field tended to be homogeneous over the MASP and the average wind in this period was weak.

3.2.2. Increase in Ozone Concentration in All Station (7E)

In the 7E case (Figure 9), the model represented the nocturnal increase in ozone, although in most seasons, an underestimation occurred (difference of almost $30 \mu\text{g m}^{-3}$). At DIAD and Parque Dom Pedro II (PDP2) stations, although the nocturnal increase in ozone was represented, there was a lag in the model's concentration and that obtained in such stations. Regarding daytime maximums, there was an overestimation for both days at all points analyzed. The average ozone field for this simulation (Figure 10) showed values below $24 \mu\text{g m}^{-3}$ in the continental part and a core of maximum values southwest of the domain, where the wind tends to have a higher average intensity when compared to the rest of the study area. The ozone increase in all air quality stations was associated with the summer period in the south hemisphere, which provides higher temperatures and higher incidence of solar radiation during daytime [39]. For the MASP, Carvalho et al. [40] associated the increase in nocturnal ozone with possible horizontal and vertical transport from other regions and the trapped pollutant in higher levels in the atmosphere.

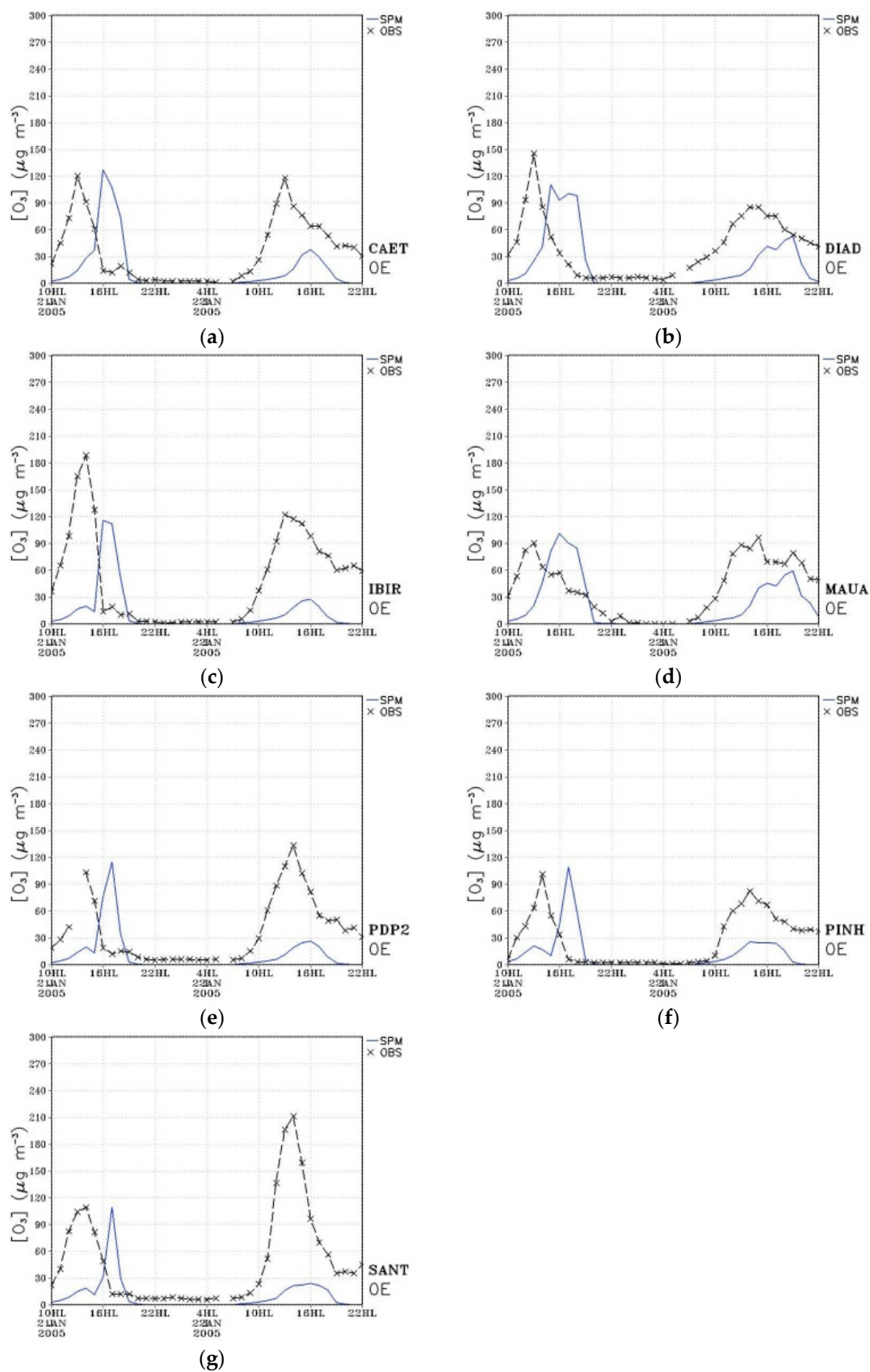


Figure 7. Ozone concentration (in $\mu\text{g m}^{-3}$ and local time-HL) of observed (OBS, dashed line with x symbol) and simulated (SPM, continuous line) at (a) São Caetano do Sul (CAET), (b) Diadema (DIAD), (c) Ibirapuera Park (IBIR), (d) Mauá (MAUA), (e) Pq. D. Pedro II (PDP2), (f) Pinheiros (PINH) and (g) Santana (SANT). Simulation for 0E case.

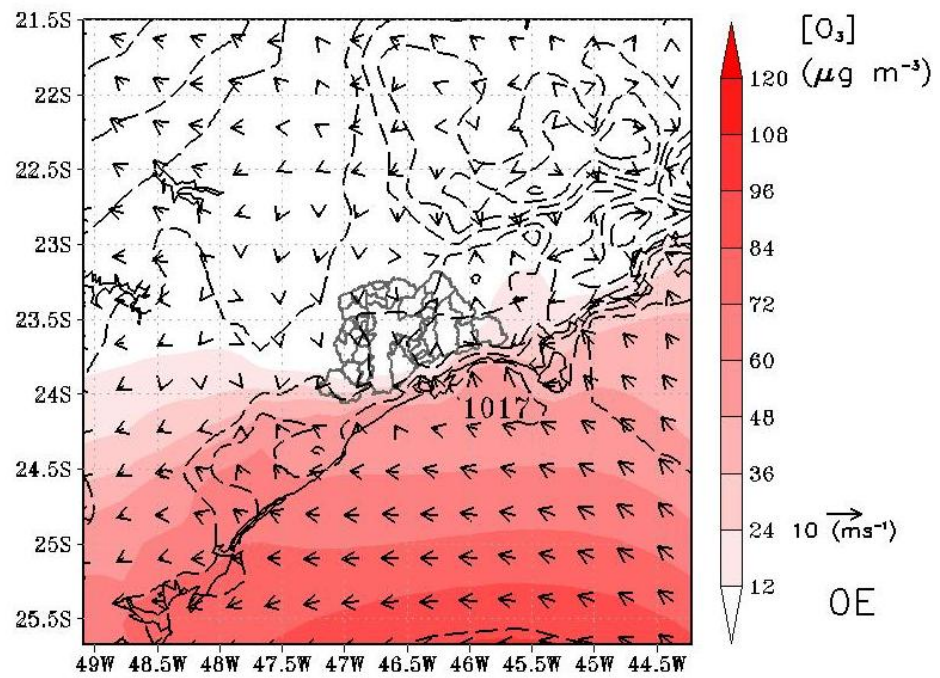


Figure 8. Average ozone concentration (color bar, in $\mu\text{g m}^{-3}$), reduced pressure at average sea level (hPa), and average wind (m s^{-1}) for the corresponding period between 22 HL and 10 HL (local time) at the first output level of the model. Simulation for OE case.

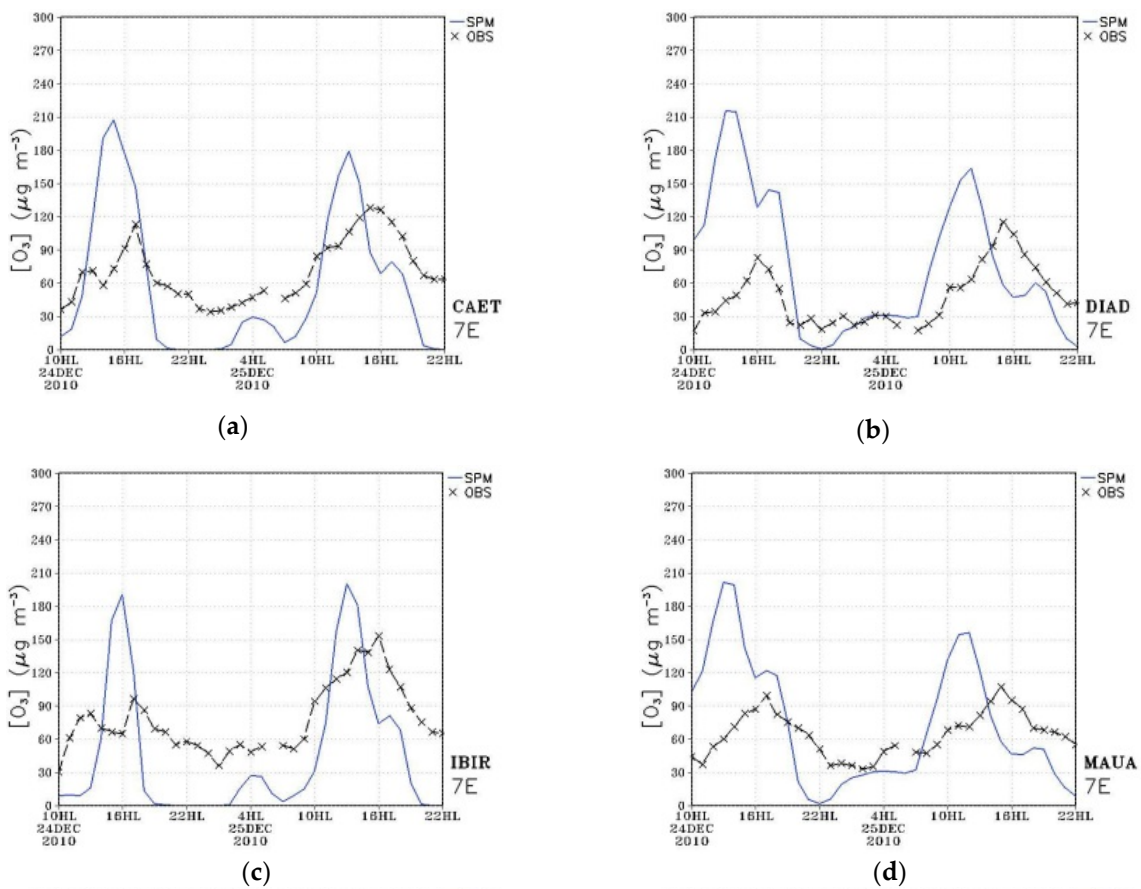


Figure 9. Cont.

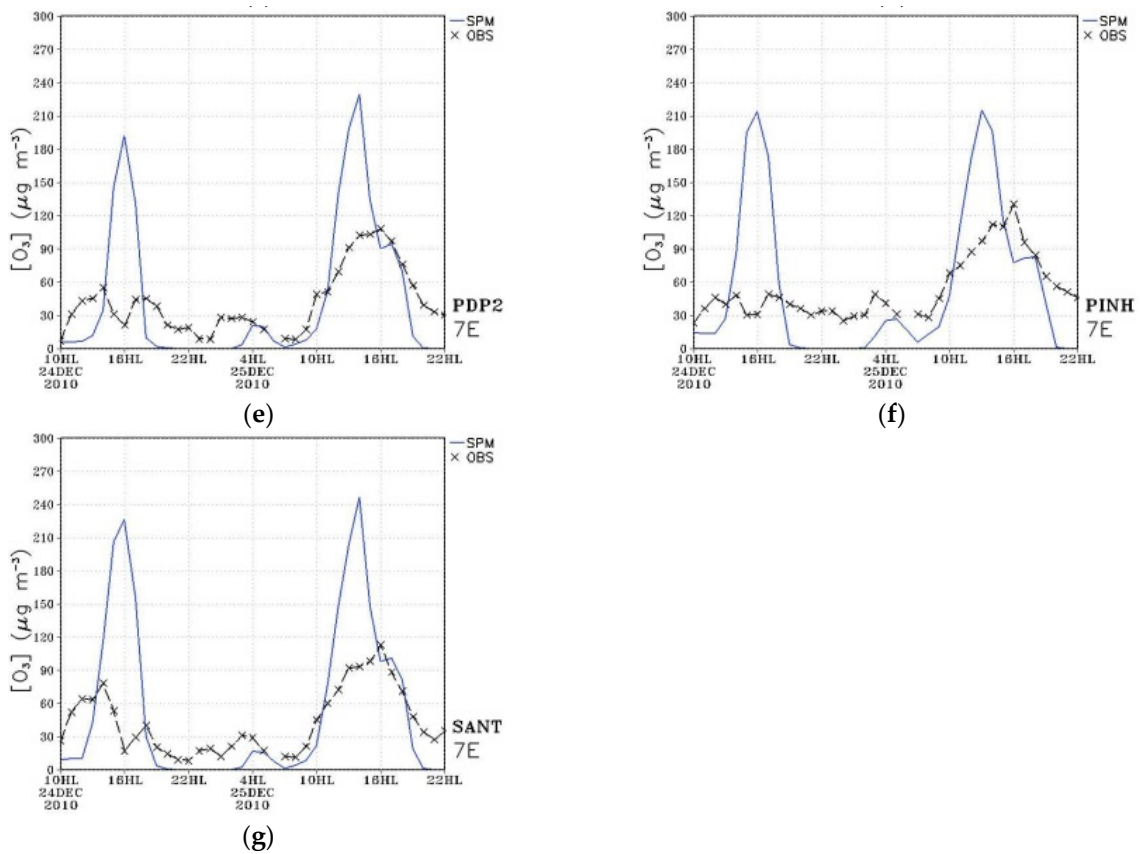


Figure 9. Ozone concentration (in $\mu\text{g m}^{-3}$ and local time, HL) observed (OBS, dashed line with x symbol) and simulated (SPM, continuous line) at (a) São Caetano do Sul (CAET), (b) Diadema (DIAD), (c) Ibirapuera Park (IBIR), (d) Mauá (MAUA), (e) Pq. D. Pedro II (PDP2), (f) Pinheiros (PINH) and (g) Santana (SANT). Simulation for 7E case.

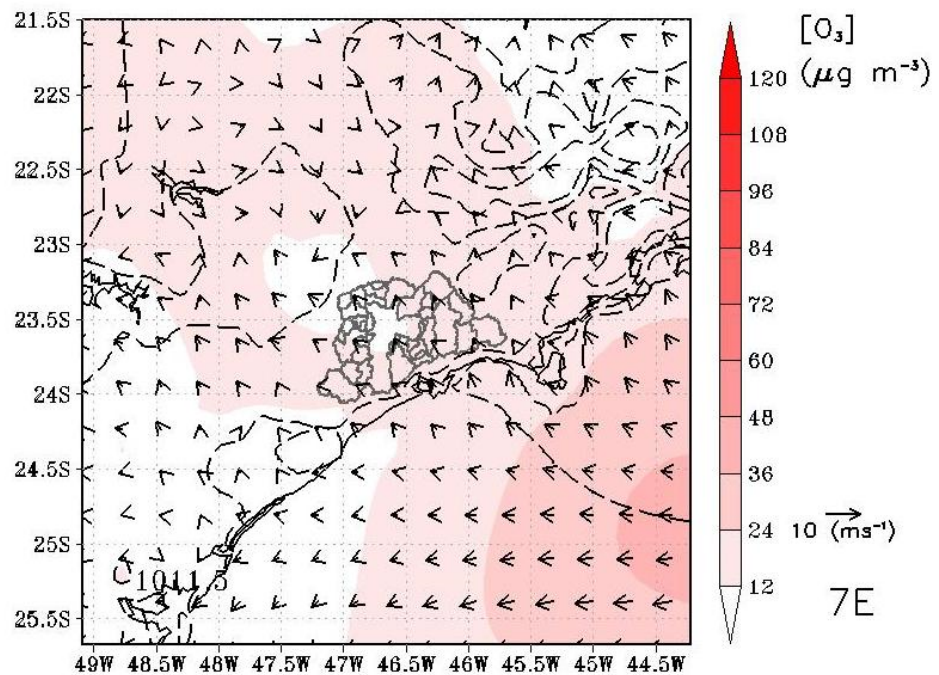


Figure 10. Average ozone concentration (color bar, in $\mu\text{g m}^{-3}$), reduced pressure at average sea level (hPa), and average wind (m s^{-1}) or the corresponding period between 22:00 HL and 10:00 HL (local time) at the first output level of the model. Simulation for 7E case.

3.2.3. Increase in Ozone Concentration in Some Stations (GP)

Although in the GP case (Figure 11) the model simulated concentrations closer to the values observed in the stations, the behavior of ozone at night was not accurately represented. At DIAD and MAUA stations, the model simulated the night peak, but its maximum value was out of step with the observed value. At the CAET station, the model could not reproduce the nocturnal ozone increase. In Figure 12, low concentration values were observed in the central and northwest region of the MASP, coinciding with the location of the CAET, PDP2, Pinheiros (PINH), and Ibirapuera Park (IBIR) stations. The minimal ozone concentration in this area is associated with the depletion by other pollutant emissions in the MASP [38,41]. Slightly higher values (but below $24 \mu\text{g m}^{-3}$) in the periphery, as in case 7E, may be associated with a localized increase due to the mostly vertical transport of this pollutant [40].

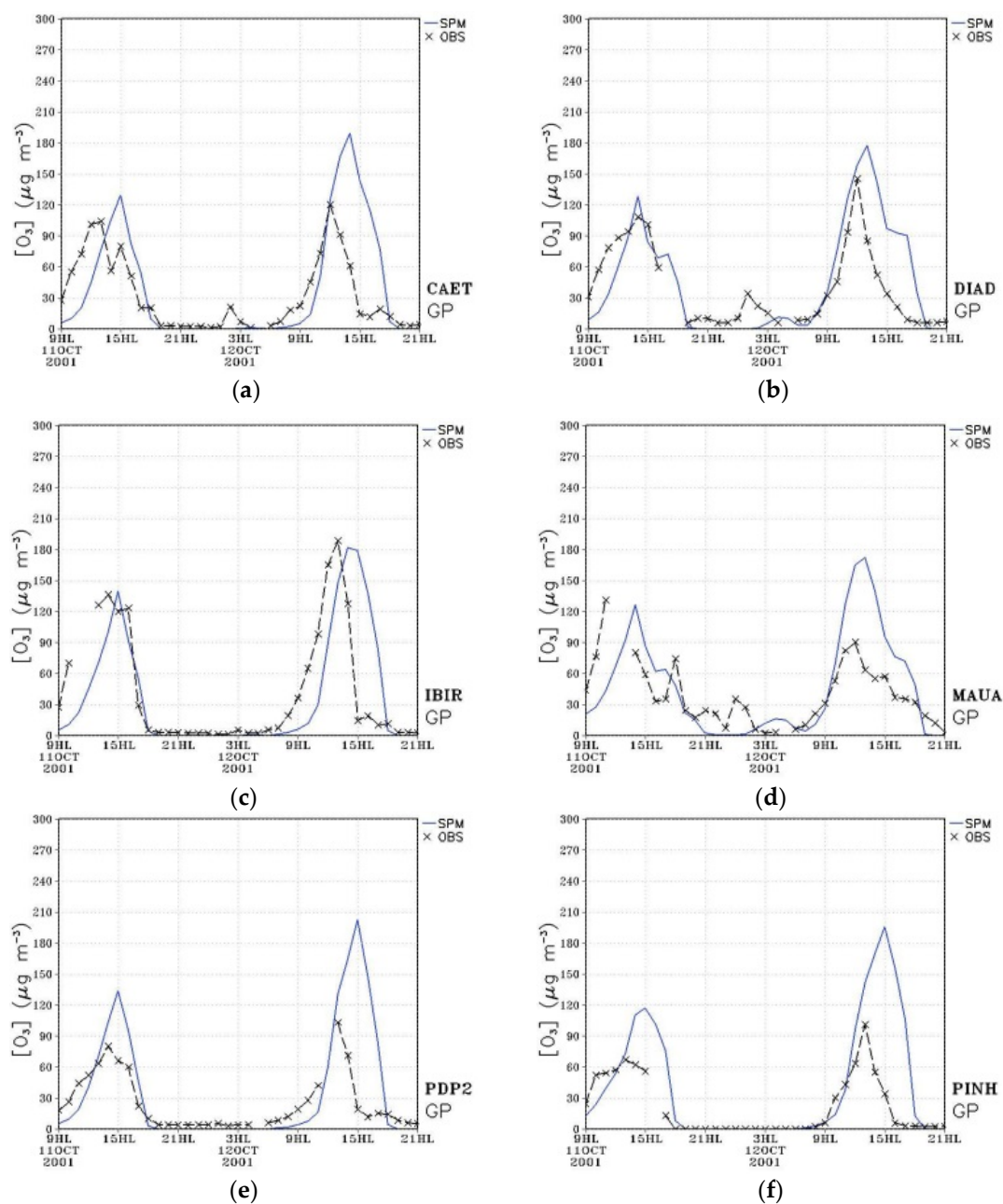


Figure 11. Cont.

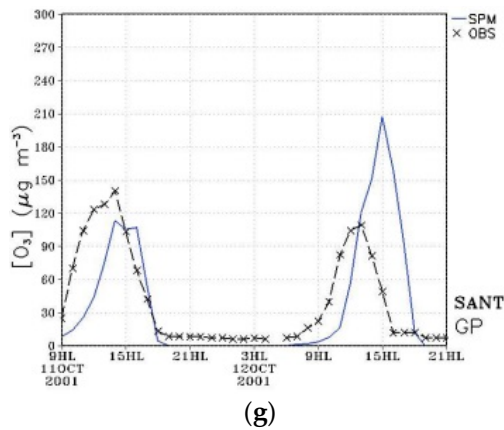


Figure 11. Ozone concentration (in $\mu\text{g m}^{-3}$ and local time, HL) observed (OBS, dashed line with x symbol) and simulated (SPM, continuous line) at (a) São Caetano do Sul (CAET), (b) Diadema (DIAD), (c) Ibirapuera Park (IBIR), (d) Mauá (MAUA), (e) Pq. D. Pedro II (PDP2), (f) Pinheiros (PINH) and (g) Santana (SANT). Simulation for GP case.

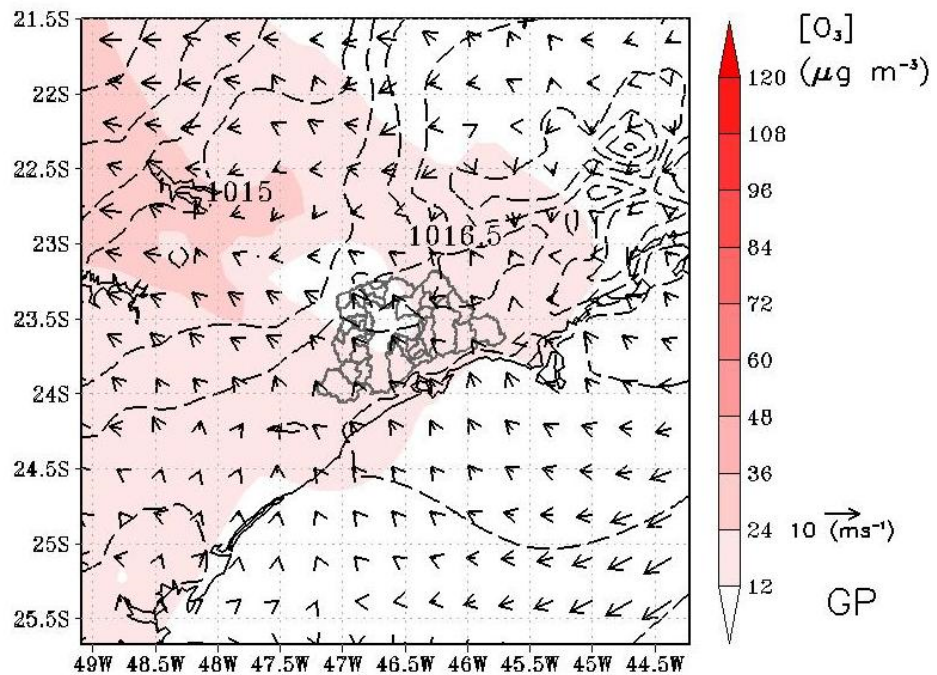


Figure 12. Average ozone concentration (color bar, in $\mu\text{g m}^{-3}$), reduced pressure at average sea level (hPa), and average wind (m s^{-1}) for the corresponding period between 22:00 HL and 10:00 HL (local time) at the first output level of the model. Simulation for GP case.

3.2.4. Ozone Vertical Profile

In case 0E (Figure 13), the wind remained weak throughout the period, with a minimal vertical component. The atmosphere under the MASP was clean for all hours of the night. When an increase in the ozone concentration was observed in all stations in the MASP (case 7E, Figure 14), the sub-wind component was more intense than when this phenomenon was observed in only a few stations (case GP, Figure 15). In this case (Figure 15), ozone was concentrated in the residual layer, with higher concentration values between 500 to 1000 m and further away to the west of the urban area. A subsidence component of the wind was observed at levels close to the surface, although weak, in the city’s eastern region, contributing to the transport of ozone from the upper layers. This result shows that, in the cases of the nocturnal peak, the vertical transport of ozone present in the residual layer has an essential contribution in the generation of increased concentration at levels close to the surface.

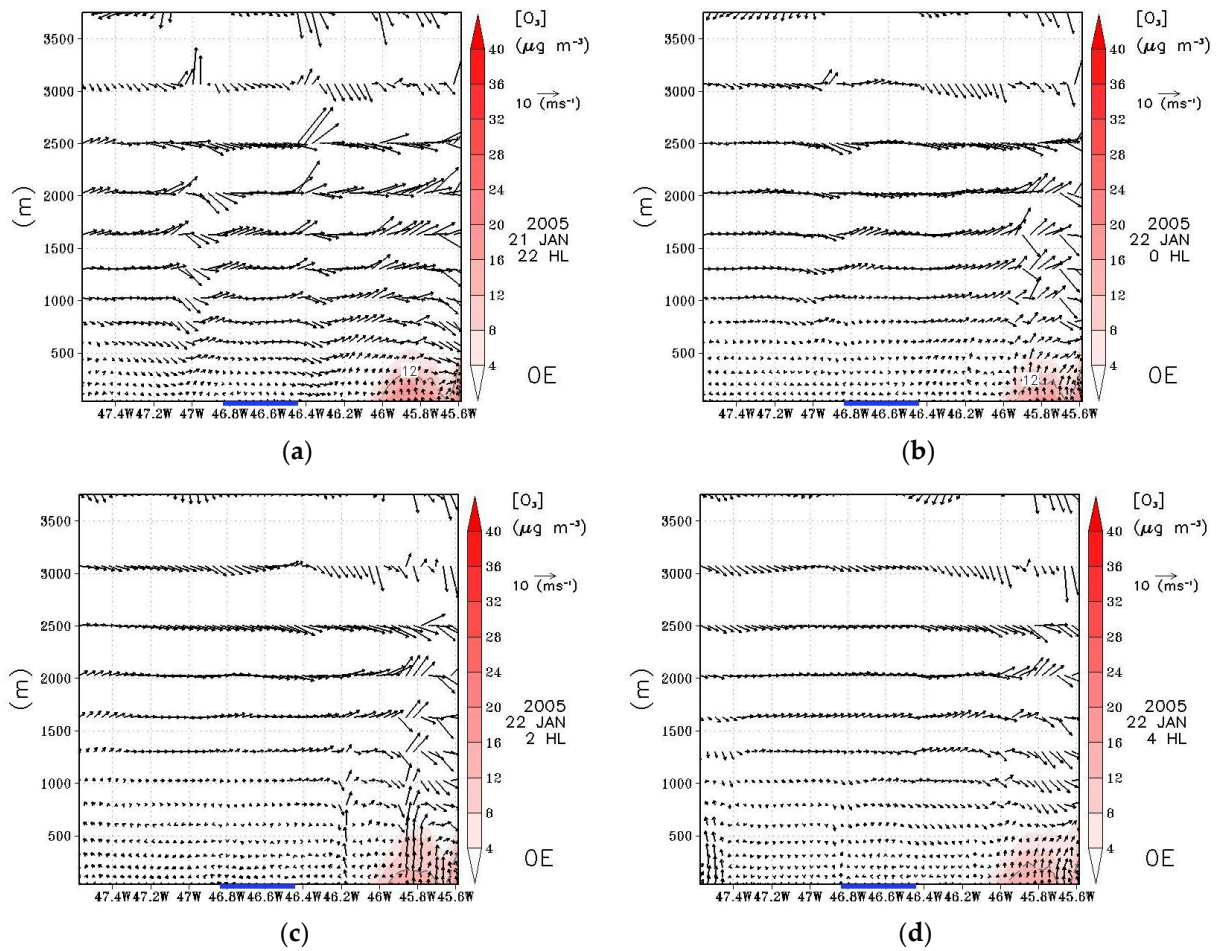


Figure 13. Ozone concentration ($\mu\text{g m}^{-3}$) and vertical wind component (m s^{-1}) with the zonal wind (m s^{-1}) for a vertical view at 23.616° S latitude, for the case 0E. The blue line indicates the location of the MASP. Local time is indicated in the corresponding figure (a) 22 HL; (b) 0 HL; (c) 2 HL; (d) 4 HL.

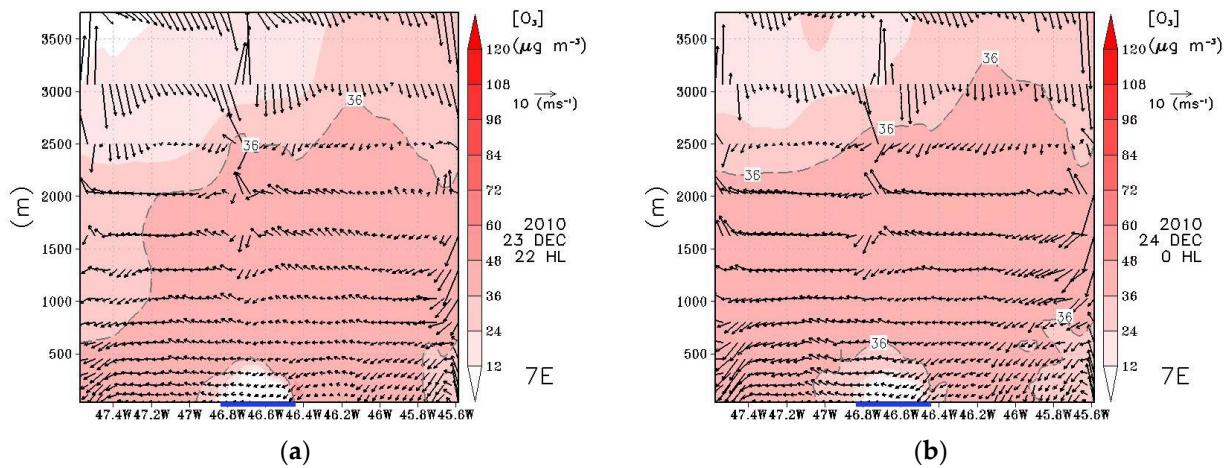


Figure 14. Cont.

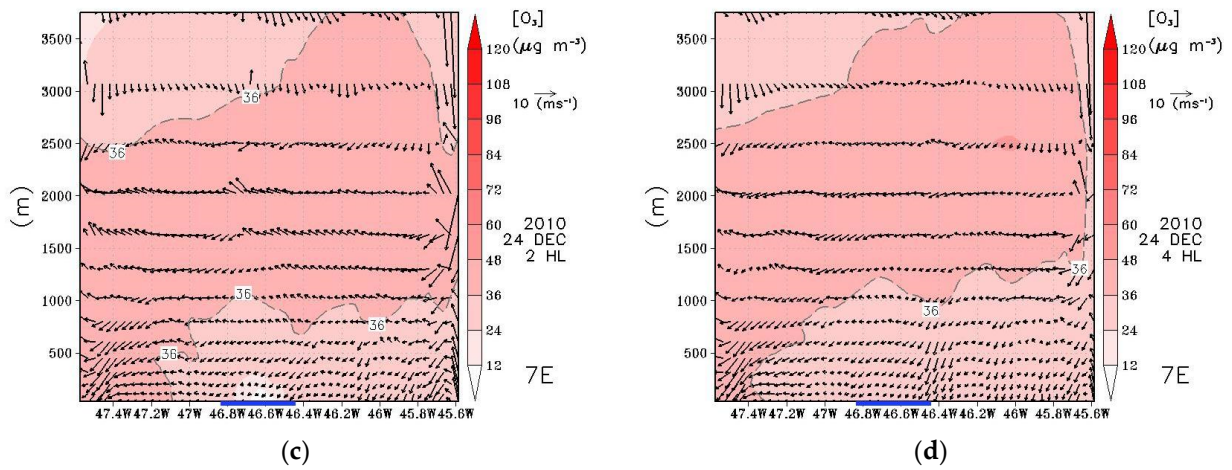


Figure 14. Ozone concentration ($\mu\text{g m}^{-3}$) and vertical wind component (m s^{-1}) with the zonal wind (m s^{-1}) for a vertical view at 23.616° S latitude, for the case 7E. The blue line indicates the location of the MASP. Local time is indicated in the corresponding figure (a) 22 HL; (b) 0 HL; (c) 2 HL; (d) 4 HL.

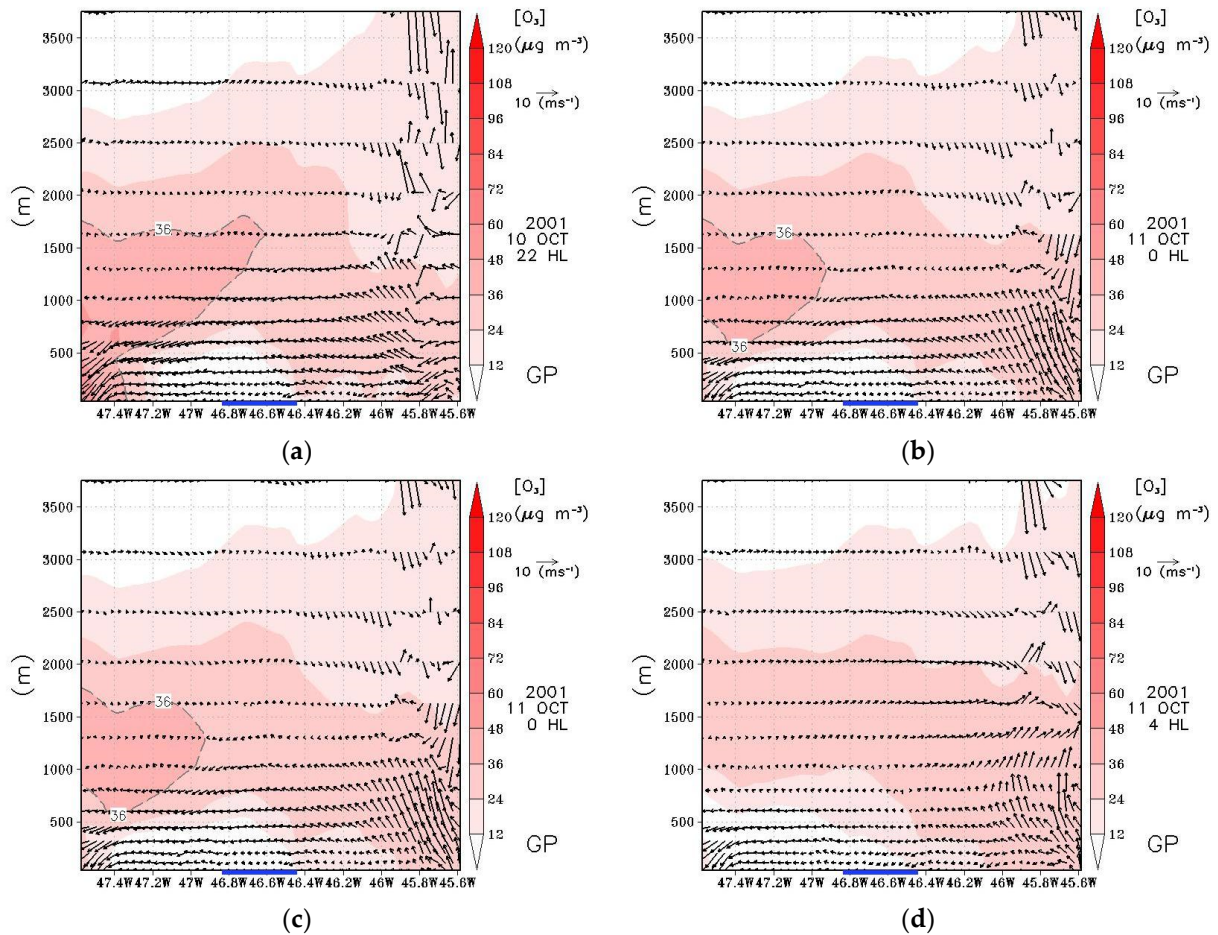


Figure 15. Ozone concentration ($\mu\text{g m}^{-3}$) and vertical wind component (m s^{-1}) with the zonal wind (m s^{-1}) for a vertical view at 23.616° S latitude, for the case GP. The blue line indicates the location of the MASP. Local time is indicated in the corresponding figure. (a) 22 HL; (b) 0 HL; (c) 0 HL; (d) 4 HL.

4. Conclusions and Remarks

To study the local characteristics that contribute to an increase in ozone concentrations at nighttime in the MASP, three cases were simulated: when no increase was observed (0E), when the increase was observed in some stations (GP), and when the secondary peak was observed in all air quality stations (7E). In general, the model represented the nocturnal evolution of ozone concentrations close to the surface at stations located in the MASP. For daytime concentrations, the model overestimated the simulated maximum values. The atmospheric condition resulting from the simulations for the MASP was similar for the three simulations, confirming that the formation of nightly ozone peaks is not linked to the synoptic situation in this study region. In this case, the most significant influence resides in the amount of ozone trapped in the residual layer and the intensity of the subsiding currents over the urban area, as seen in the vertical sections for all cases.

Author Contributions: All authors have contributed equally. All authors have read and agreed to the published version of the manuscript.

Funding: The authors would like to thank the financial support of the Coordenação de Aperfeiçoamento de Pessoal de Nível (CAPES) and the São Paulo Research Foundation (Grants number 2011/01040-0, 2016/18438-0, and 2017/17047-0).

Acknowledgments: The authors would like to thank CETESB for openly sharing the air quality data.

Conflicts of Interest: The authors declare no conflict of interest.

References

1. Manisalidis, I.; Stavropoulou, E.; Stavropoulos, A.; Bezirtzoglou, E. Environmental and Health Impacts of Air Pollution: A Review. *Front. Public Health* **2020**, *8*, 1–13. [[CrossRef](#)]
2. Patz, J.A.; Campbell-Lendrum, D.; Holloway, T.; Foley, J.A. Impact of regional climate change on human health. *Nature* **2005**, *438*, 310–317. [[CrossRef](#)]
3. Woodall, G.M.; Hoover, M.D.; Williams, R.; Benedict, K.; Harper, M.; Soo, J.C.; Jarabek, A.M.; Stewart, M.J.; Brown, J.S.; Hulla, J.E.; et al. Interpreting mobile and handheld air sensor readings in relation to air quality standards and health effect reference values: Tackling the challenges. *Atmosphere* **2017**, *8*, 182. [[CrossRef](#)]
4. Bell, M.L.; Zanobetti, A.; Dominici, F. Who is More Affected by Ozone Pollution? A Systematic Review and Meta-Analysis. *Am. J. Epidemiol.* **2014**, *180*, 15–28. [[CrossRef](#)] [[PubMed](#)]
5. Liana, M.; Edison, O.; Jorge, M.; Marcos, M.; Leda, A.; Guerrero, U.; Leila, M.D. Current state of air quality in major cities of Latin America. *Ciência Nat.* **2016**, *38*, 523–531. [[CrossRef](#)]
6. Peláez, L.M.G.; Santos, J.M.; Albuquerque, T.T.d.A.; Reis, N.C.; Andreão, W.L.; Andrade, M.d.F. Air quality status and trends over large cities in South America. *Environ. Sci. Policy* **2020**, *114*, 422–435. [[CrossRef](#)]
7. Han, L.; Zhou, W.; Pickett, S.T.A.; Li, W.; Li, L. An optimum city size? the scaling relationship for urban population and fine particulate (PM_{2.5}) concentration. *Environ. Pollut.* **2016**, *208*, 96–101. [[CrossRef](#)] [[PubMed](#)]
8. Wang, T.; Kwok, J.Y.H. Measurement and Analysis of a Multiday Photochemical Smog Episode in the Pearl River Delta of China. *J. Appl. Meteorol.* **2003**, *42*, 404–416. [[CrossRef](#)]
9. Andrade, M.D.F.; Ynoue, R.Y.; Freitas, E.D.; Todesco, E.; Vela, A.V.; Ibarra, S.; Martins, L.D.; Martins, J.A.; Carvalho, V.S.B. Air quality forecasting system for Southeastern Brazil. *Front. Environ. Sci.* **2015**, *3*, 1–14. [[CrossRef](#)]
10. Samaali, M.; Moran, M.D.; Bouchet, V.S.; Pavlovic, R.; Cousineau, S.; Sassi, M. On the influence of chemical initial and boundary conditions on annual regional air quality model simulations for North America. *Atmos. Environ.* **2009**, *43*, 4873–4885. [[CrossRef](#)]
11. Balzarini, A.; Pirovano, G.; Honzak, L.; Žabkar, R.; Curci, G.; Forkel, R.; Hirtl, M.; San José, R.; Tuccella, P.; Grell, G.A. WRF-Chem model sensitivity to chemical mechanisms choice in reconstructing aerosol optical properties. *Atmos. Environ.* **2015**, *115*, 604–619. [[CrossRef](#)]
12. Vara-Vela, A.; Andrade, M.F.; Kumar, P.; Ynoue, R.Y.; Muñoz, A.G. Impact of vehicular emissions on the formation of fine particles in the Sao Paulo Metropolitan Area: A numerical study with the WRF-Chem model. *Atmos. Chem. Phys.* **2016**, *16*, 777–797. [[CrossRef](#)]
13. Mateos, A.C.; Amarillo, A.C.; Busso, I.T.; Carreras, H.A. Influence of Meteorological Variables and Forest Fires Events on Air Quality in an Urban Area (Córdoba, Argentina). *Arch. Environ. Contam. Toxicol.* **2019**, *77*, 171–179. [[CrossRef](#)] [[PubMed](#)]
14. Romero, H.; Ihl, M.; Rivera, A.; Zalazar, P.; Azocar, P. Rapid urban growth, land-use changes and air pollution in Santiago, Chile. *Atmos. Environ.* **1999**, *33*, 4039–4047. [[CrossRef](#)]
15. Mar, K.A.; Ojha, N.; Pozzer, A.; Butler, T.M. Ozone air quality simulations with WRF-Chem (v3.5.1) over Europe: Model evaluation and chemical mechanism comparison. *Geosci. Model Dev.* **2016**, *9*, 3699–3728. [[CrossRef](#)]

16. Ren, X.; Mi, Z.; Georgopoulos, P.G. Comparison of Machine Learning and Land Use Regression for fine scale spatiotemporal estimation of ambient air pollution: Modeling ozone concentrations across the contiguous United States. *Environ. Int.* **2020**, *142*, 105827. [CrossRef]
17. Gramsch, E.; Cereceda-Balic, F.; Oyola, P.; von Baer, D. Examination of pollution trends in Santiago de Chile with cluster analysis of PM10 and Ozone data. *Atmos. Environ.* **2006**, *40*, 5464–5475. [CrossRef]
18. Khan, B.A.; de Freitas, C.R.; Shooter, D. Application of synoptic weather typing to an investigation of nocturnal ozone concentration at a maritime location, New Zealand. *Atmos. Environ.* **2007**, *41*, 5636–5646. [CrossRef]
19. Alp, K.; Hanedar, A.O. Determination of transport processes of nocturnal ozone in Istanbul atmosphere. *Int. J. Environ. Pollut.* **2009**, *39*, 213. [CrossRef]
20. Zhu, X.; Ma, Z.; Li, Z.; Wu, J.; Guo, H.; Yin, X.; Ma, X.; Qiao, L. Impacts of meteorological conditions on nocturnal surface ozone enhancement during the summertime in Beijing. *Atmos. Environ.* **2020**, *225*, 117368. [CrossRef]
21. Ghosh, D.; Lal, S.; Sarkar, U. High nocturnal ozone levels at a surface site in Kolkata, India: Trade-off between meteorology and specific nocturnal chemistry. *Urban Clim.* **2013**, *5*, 82–103. [CrossRef]
22. Godowitch, J.M.; Gilliland, A.B.; Draxler, R.R.; Rao, S.T. Modeling assessment of point source NOx emission reductions on ozone air quality in the eastern United States. *Atmos. Environ.* **2008**, *42*, 87–100. [CrossRef]
23. Sicard, P.; Serra, R.; Rossello, P. Spatiotemporal trends in ground-level ozone concentrations and metrics in France over the time period 1999–2012. *Environ. Res.* **2016**, *149*, 122–144. [CrossRef] [PubMed]
24. IBGE Censo Demográfico: Características da População—Amostra. Available online: <https://censo2010.ibge.gov.br/resultados.html> (accessed on 16 October 2020).
25. Nair, K.N.; Freitas, E.D.; Sánchez-Ccoyllo, O.R.; Silva Dias, M.a.F.; Silva Dias, P.L.; Andrade, M.F.; Massambani, O. Dynamics of urban boundary layer over São Paulo associated with mesoscale processes. *Meteorol. Atmos. Phys.* **2004**, *86*, 87–98. [CrossRef]
26. Andrade, M.d.F.; Kumar, P.; de Freitas, E.D.; Ynoue, R.Y.; Martins, J.; Martins, L.D.; Nogueira, T.; Perez-Martinez, P.; de Miranda, R.M.; Albuquerque, T.; et al. Air quality in the megacity of São Paulo: Evolution over the last 30 years and future perspectives. *Atmos. Environ.* **2017**, *159*, 66–82. [CrossRef]
27. Freitas, S.R.; Panetta, J.; Longo, K.M.; Rodrigues, L.F.; Moreira, D.S.; Rosário, N.E.; Silva Dias, P.L.; Silva Dias, M.A.F.; Souza, E.P.; Freitas, E.D.; et al. The Brazilian developments on the Regional Atmospheric Modeling System (BRAMS 5.2): An integrated environmental model tuned for tropical areas. *Geosci. Model Dev.* **2017**, *10*, 189–222. [CrossRef] [PubMed]
28. Cotton, W.R.; Pielke, R.A., Sr.; Walko, R.L.; Liston, G.E.; Tremback, C.J.; Jiang, H.; McAnelly, R.L.; Harrington, J.Y.; Nicholls, M.E.; Carrio, G.G.; et al. RAMS 2001: Current status and future directions. *Meteorol. Atmos. Phys.* **2003**, *82*, 5–29. [CrossRef]
29. Walko, R.L.; Band, L.E.; Baron, J.; Kittel, T.G.F.; Lammers, R.; Lee, T.J.; Ojima, D.; Pielke, R.A.; Taylor, C.; Tague, C.; et al. Coupled Atmosphere–Biophysics–Hydrology Models for Environmental Modeling. *J. Appl. Meteorol.* **2000**, *39*, 931–944. [CrossRef]
30. Masson, V. A physically-based scheme for the urban energy budget in atmospheric models. *Bound. Layer Meteorol.* **2000**, *94*, 357–397. [CrossRef]
31. Daley, R. (Ed.) *Atmospheric Data Analysis*; Cambridge University Press: Cambridge, UK, 1991.
32. Morais, M.V.B.; Freitas, E.D.; Marciotto, E.R.; Guerrero, V.V.U.; Martins, L.D.; Martins, J.A. Implementation of observed sky-view factor in a mesoscale model for sensitivity studies of the urban meteorology. *Sustainability* **2018**, *10*, 2183. [CrossRef]
33. Freitas, E.D.; Martins, L.D.; Silva Dias, P.L.; Andrade, M.F. A simple photochemical module implemented in RAMS for tropospheric ozone concentration forecast in the metropolitan area of São Paulo, Brazil: Coupling and validation. *Atmos. Environ.* **2005**, *39*, 6352–6361. [CrossRef]
34. Wang, L.; Zhang, Y.; Wang, K.; Zheng, B.; Zhang, Q.; Wei, W. Application of Weather Research and Forecasting Model with Chemistry (WRF/Chem) over northern China: Sensitivity study, comparative evaluation, and policy implications. *Atmos. Environ.* **2014**. [CrossRef]
35. Morais, M.V.B.; de Freitas, E.D.; Guerrero, V.V.U.; Martins, L.D. A modeling analysis of urban canopy parameterization representing the vegetation effects in the megacity of São Paulo. *Urban Clim.* **2016**, *17*, 102–115. [CrossRef]
36. CETESB. *Qualidade do Ar no Estado de São Paulo 2010*; CETESB: São Paulo, Brazil, 2011.
37. Kalnay, E.; Kanamitsu, M.; Kistler, R.; Collins, W.; Deaven, D.; Gandin, L.; Iredell, M.; Saha, S.; White, G.; Woollen, J.; et al. The NCEP/NCAR 40-year reanalysis project. *Bull. Am. Meteorol. Soc.* **1996**, *77*, 437–472. [CrossRef]
38. Franco, D.M.P.; Andrade, M.d.F.; Ynoue, R.Y.; Ching, J. Effect of Local Climate Zone (LCZ) classification on ozone chemical transport model simulations in Sao Paulo, Brazil. *Urban Clim.* **2019**, *27*, 293–313. [CrossRef]
39. Martins, L.D.; Wikuats, C.F.H.; Capucim, M.N.; Almeida, D.S.; Costa, S.C.; Albuquerque, T.; Barreto Carvalho, V.S.; Freitas, E.D.; de Fátima Andrade, M.; Martins, J.A. Extreme value analysis of air pollution data and their comparison between two large urban regions of South America. *Weather Clim. Extrem.* **2017**, *18*, 44–54. [CrossRef]
40. Carvalho, V.S.B.; Freitas, E.D.; Martins, L.D.; Martins, J.A.; Mazzoli, C.R.; de Fátima Andrade, M. Air quality status and trends over the Metropolitan Area of São Paulo, Brazil as a result of emission control policies. *Environ. Sci. Policy* **2015**, *47*, 68–79. [CrossRef]
41. Alvim, D.S.; Gatti, L.V.; Corrêa, S.M.; Chiquetto, J.B.; Santos, G.M.; de Souza Rossatti, C.; Pretto, A.; Rozante, J.R.; Figueroa, S.N.; Pendharkar, J.; et al. Determining VOCs reactivity for ozone forming potential in the megacity of São Paulo. *Aerosol Air Qual. Res.* **2018**, *18*, 2460–2474. [CrossRef]